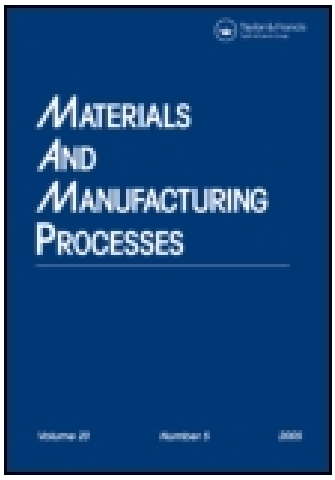

Materials and Manufacturing Processes
Publication details, including instructions for authors and subscription information:
http://www.tandfonline.com/loi/lmmp20

Constrained Efficient Global Optimization for Pultrusion Process

Cem C. Tutum[a], Kalyanmoy Deb[a] & Ismet Baran[b]
[a] Department of Electrical and Computer Engineering, Michigan State University, East Lansing, MI, USA
[b] Faculty of Engineering Technology, Chair of Production Technology, University of Twente, Enschede, The Netherlands
Accepted author version posted online: 20 Dec 2014.

To cite this article: Cem C. Tutum, Kalyanmoy Deb & Ismet Baran (2015) Constrained Efficient Global Optimization for Pultrusion Process, Materials and Manufacturing Processes, 30:4, 538-551, DOI: 10.1080/10426914.2014.994752

To link to this article: http://dx.doi.org/10.1080/10426914.2014.994752

Materials and Manufacturing Processes, 30: 538–551, 2015

ISSN: 1042-6914 print/1532-2475 online
DOI: 10.1080/10426914.2014.994752

Taylor & Francis
Taylor & Francis Group

Constrained Efficient Global Optimization for Pultrusion Process

Cem C. Tutum[1], Kalyanmoy Deb[1], and Ismet Baran[2]

[1]*Department of Electrical and Computer Engineering, Michigan State University, East Lansing, MI, USA*
[2]*Faculty of Engineering Technology, Chair of Production Technology, University of Twente, Enschede, The Netherlands*

Composite materials, as the name indicates, are composed of different materials that yield superior performance as compared to individual components. Pultrusion is one of the most cost-effective manufacturing techniques for producing fiber-reinforced composites with constant cross-sectional profiles. This obviously makes it more attractive for both researchers and practitioners to investigate the optimum process parameters. Validated computer simulations cost less as compared to physical experiments, therefore this makes them an efficient tool for numerical optimization. However, the complexity of the numerical models can still be "expensive" and forces us to use them sparingly. These relatively more complex models can be replaced with "surrogates," which are less complex and are therefore faster to evaluate representative models. In this article, a previously validated thermochemical simulation of the pultrusion process has shortly been presented. Following this, a new constrained optimization methodology based on a well-known surrogate method, i.e., Kriging, is introduced. Next, a validation case is presented to clarify the working principles of the implementation, which also supports the upcoming main optimization test cases. This design problem involves the design of the heating die with one, two, and three heaters together with the pulling speed. The results show that the proposed methodology is very efficient in finding the optimal process and design parameters.

Keywords Composites; Constraint handling; Curing; Global optimization; Kriging; Pultrusion; Surrogate; Thermochemical simulation.

Introduction

Pultrusion is one of the most cost-effective manufacturing techniques for producing fiber-reinforced composites with constant cross-sectional profiles. A schematic view of the process setup is shown in Fig. 1. The reinforcement is most often fiberglass; however, carbon fiber, aramid, or mixture can also be used. The reinforcement material is pulled and guided through a resin impregnation system, which can be either open resin bath or resin injection chamber. The fiber reinforcement is fully wetted out such that all the fibers are saturated in the resin. The reinforcements and the resin pass through a heated die once the resin impregnates the reinforcement material. Inside the heated die, the state of the resin gradually changes from liquid to solid because of the exothermic reaction of the thermosetting resin. The cured and solidified product is pulled via a pulling mechanism, and at the end of the process is cut to the desired length.

In order to have a better understanding for the thermochemical aspects of the process, several studies have been investigated related to the numerical modeling of the pultrusion process in the literature [1–10]. In the thermochemical analysis, the evolution of the temperature and the degree of cure inside the heated die has been predicted during the process. The effects of the thermal contact resistance (TCR) at the die–part interface on the pultrusion process of a composite rod have been investigated by using the control volume-based finite difference (CV/FD) method in [6], and it was found that the use of a variable TCR is more reliable than the use of a constant TCR for the simulation of the process. In the work [7], three-dimensional (3D) numerical modeling strategies of a thermosetting pultrusion process were investigated considering both transient and steady-state approaches. For the transient solution, an unconditionally stable alternating direction implicit Douglas–Gunn (ADI-DG) scheme was implemented. The process-induced residual stresses and distortions have been predicted in [8]. It was found that tension stresses prevail at the end of the process for the inner region of the composite since the curing rate is higher here as compared to the outer regions where compressive stresses are obtained. The separation between the heating die and the part due to shrinkage was also investigated using a mechanical contact formulation at the die–part interface.

Having given an overview about the general activities and challenges about the multi-physics simulation of the pultrusion process, it is worth here to note that the evaluation of these manufacturing process simulations brings with them long waiting hours due to their computationally intensive nature [11]. This inherently motivates the desire to exploit the efficient and cheaper approximating methods which are called as surrogates, meta-models, or response surfaces in mathematical parlance [12–16]. Most known surrogates in the literature vary from simple polynomial regression models and moving least squares to neural networks [17–19], radial basis functions, Kriging, and support vector regression [20]. Some of these methods are listed under machine learning, statistical learning, or in general supervised learning

Received June 13, 2014; Accepted November 7, 2014

Address correspondence to Cem C. Tutum, Department of Electrical and Computer Engineering, Michigan State University, East Lansing, MI 48824, USA; E-mail: tutum@msu.edu

Color versions of one or more of the figures in the article can be found online at www.tandfonline.com/lmmp.

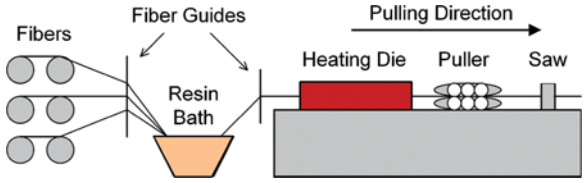

FIGURE 1.—Schematic view of the pultrusion process.

techniques. Despite the variety in their mathematical construction, they all work on the same consecutive principles: training (learning) and testing (prediction or generalization). Training, in simple terms, is the procedure of learning the behavior of the underlying response as a function of some chosen parameters, which can also be called as the mathematical mapping. Once this mapping is learned considering limited sample size, e.g., in case of using multidisciplinary manufacturing process simulations, it can be replaced with the computationally expensive black-box function. This simpler model allows the user to predict any response at an unknown design set at a negligible cost. However, the sample size easily fall short with respect to the number of unknowns as well as the competing combinations of them in engineering design problems [20]. At this point, reminding the fact that the main purpose of constructing the surrogate is to use it within a proper search strategy. The surrogate-based optimization strategies can be grouped into three subclasses: (i) exploitation-based techniques, (ii) exploration-based techniques, and (iii) balanced techniques which combine the first two. The first group of algorithms is constructed with an emphasis of finding a local optimum of the predictor; however, the uncertainty in the surrogate built upon the limited number of samples is overlooked at the first place which results in high probability of premature convergence. On the other hand, the second group of surrogate-based optimization algorithms puts more emphasis on exploring the design space, thereby reducing the uncertainty in the surrogate, which inevitably makes them slower but more robust as compared to the first group of algorithms. As expected from the course of this discussion, the most important challenge is obviously to construct an algorithm which balances both goals by letting the algorithm to explore the search space sufficiently but at the same time avoiding waste of resources and finally reach the global optimum. Efficient global optimization (EGO), popularized by the work of Jones et al. [21] and developed by many others, is such an algorithm composed of two iterative stages: (1) construction of the surrogate and (2) employing an optimization procedure following a balanced infill criterion.

The remainder of the article is organized as follows. The section "Thermochemical Analysis" introduces the numerical model in which the energy equations and the particular solution technique employed as part of the thermochemical analysis of the pultrusion process are given. The section "Surrogate Model: Kriging" presents the surrogate model, i.e., Kriging, gives an overview of the standard EGO algorithm, and then details the new constrained EGO algorithm proposed by the authors. Following the description of the process optimization problem, The section "Results and Discussions" first presents a validation case to visualize the progress of the algorithm on a two-dimensional optimization problem. Second, the main process optimization cases involving one-, two-, and three-heater cases, in which the number of design variables is varying as 7, 10, and 13, respectively, are given. Finally, the section "Conclusions" presents the concluding remarks.

MATERIALS AND METHODS

Thermochemical Analysis

The temperature and the degree of cure fields are obtained using the CV/FD method [6, 7] implemented in MATLAB mathematical computing environment. In the numerical scheme, the steady-state approach is used and the corresponding energy equations for the composite and the die are given in Eqs. (1) and (2), respectively. Here, x_3 is the pulling (axial or longitudinal) direction; x_1 and x_2 are the transverse directions.

$$\rho_{\mathrm{c}} C_{\mathrm{p,c}} \left(u \frac{\partial T}{\partial x_3} \right) = k_{x_1,\mathrm{c}} \frac{\partial^2 T}{\partial {x_1}^2} + k_{x_2,\mathrm{c}} \frac{\partial^2 T}{\partial {x_2}^2} + k_{x_3,\mathrm{c}} \frac{\partial^2 T}{\partial {x_3}^2} + q, \tag{1}$$

$$0 = k_{x_1,\mathrm{d}} \frac{\partial^2 T}{\partial {x_1}^2} + k_{x_2,\mathrm{d}} \frac{\partial^2 T}{\partial {x_2}^2} + k_{x_3,\mathrm{d}} \frac{\partial^2 T}{\partial {x_3}^2}, \tag{2}$$

where T is the temperature; u is the pulling speed; ρ is the density; C_{p} is the specific heat; and k_{x1}, k_{x2}, and k_{x3} are the thermal conductivities along x_1, x_2, and x_3 directions, respectively. The subscriptions c and d correspond to composite and die, respectively. Lumped material properties are used and assumed to be constant throughout the process. The volumetric internal heat generation (q) [W/m^3] due to the exothermic reaction of the epoxy resin can be expressed by [5]:

$$q = (1 - V_{\mathrm{f}}) \rho_{\mathrm{r}} H_{\mathrm{tr}} R_{\mathrm{r}}(\alpha, T), \tag{3}$$

where V_{f} is the fiber volume fraction, ρ_{r} is the resin density, α is the degree of cure, and H_{tr} is the total heat of reaction during the complete cure of the resin sample which is obtained by using a differential scanning calorimetry (DSC) analysis [4, 5]. $R_{\mathrm{r}}(\alpha, T)$ is the rate of degree of cure $d\alpha/dt$ defined by an Arrhenius type of relation and expressed in Eq. (4). Generally, $d\alpha/dt$ is linearly correlated with the rate of heat, $dH(t)/dt$, generated during the curing of the resin sample, as seen in Eq. (4).

$$R_{\mathrm{r}}(\alpha, T) = \frac{d\alpha}{dt} = \frac{1}{H_{\mathrm{tr}}} \frac{dH(t)}{dt} = K_0 \exp\left(-\frac{E}{RT} \right) (1 - \alpha)^n, \tag{4}$$

where K_0 is the pre-exponential constant, E is the activation energy, R is the universal gas constant, and

n is the order of reaction (kinetic exponent). K_0, E, and n can be obtained by a curve-fitting procedure applied to the experimental data evaluated using the DSC [5].

The transient time integration scheme for $d\alpha/dt$ can be derived by using the *chain rule*. Using this, the rate of the cure degree [Eq. (4)] can be expressed as:

$$\frac{d\alpha}{dt} = \frac{\partial \alpha}{\partial t} + \frac{\partial \alpha}{\partial x_3}\frac{dx_3}{dt} = \frac{\partial \alpha}{\partial t} + u\frac{\partial \alpha}{\partial x_3}, \tag{5}$$

and from Eq. (5), the steady-state relation of the resin kinetics equation can be expressed by discarding the time-dependent term as

$$R_{\mathrm{r}}(\alpha, T) = u\frac{\partial \alpha}{\partial x_3}, \tag{6}$$

where it is the expression in Eq. (3) which is used in the steady-state numerical model (i.e., Eq. (1)).

In order to obtain stable results and overcome any oscillatory behavior in the numerical implementation, the *upwind scheme* is used for the discretization of the convective terms in the energy and resin kinetics equations. The convergence limits for reaching the steady-state conditions are set to 0.001°C and 0.0001 for the temperature and the degree of cure, respectively [6, 7].

In this section, a validation analysis of the present thermochemical numerical model is performed for the pultrusion of a thick flat beam. The material of the pultruded composite is selected as unidirectional glass/epoxy system and steel is used for the die block as provided in [5]. The material properties of the composite and resin kinetic parameters are given in Tables 1 and 2 [10], respectively, and assumed to be constant. Since all the thermal boundary conditions (BCs) are assumed to be symmetric, a quarter of the pultrusion domain is considered to be used in the present study and the corresponding schematic view of this 3D model is shown in Fig. 2. The details of the parameters used in the numerical model given in Fig. 2 are listed in Table 3. The set temperature of the heaters is assumed to be constant throughout the process [6, 7]. At the symmetry surfaces, adiabatic boundaries are defined across which no heat is transmitted. The remaining exterior surfaces of the die are exposed to ambient temperature with a convective heat transfer coefficient of $10\,\mathrm{W/m^2K}$ except for those located at the heating regions. Perfect thermal contact is assumed at the die–part interface as also considered by [5, 6, 22]. The temperature and the degree of cure values of all composite nodes at the die inlet are set to the resin bath temperature 30°C and 0, respectively.

TABLE 1.—Thermal properties used in the process simulation [5, 6–9].

		ρ [kg/m^3]	Cp [J/kg K)	k_{x3} [W/m K]	k_{x1}, k_{x2} [W/m K]
Composite	$V_{\mathrm{f}} = 0.639$	2090.7	797.27	0.9053	0.5592
Steel die		7833	460	40	40

TABLE 2.—Epoxy resin kinetic parameters [5, 6–9].

H_{tr} [kJ/kg]	K_0[1/s]	E[kJ/mol]	n
324	192,000	60	1.69

The temperature and degree of cure distributions are calculated at the steady state since pultrusion is a continuous process such that the composite part entering the heating die experiences these steady-state profiles during processing. The predicted evolution of the temperature and cure degree profiles, together with the corresponding contour plots at the die exit, are depicted in Fig. 3. These profiles obtained by using the steady-state approach are also compared with the ones calculated using a transient finite element method approach in Fig. 3 (left), and it is seen that there is a good agreement between the results. This shows that the proposed numerical scheme is stable and converged to a reliable solution. It is also seen from Fig. 3 (right) that nonuniform temperature and cure degree distributions, promoting large through-thickness thermal and cure gradients, are obtained inside the heating die such that the point B cures faster than the point A. The cure degree at the die exit is calculated approximately as 0.86 and 0.90 at points A and B, respectively. The maximum temperature is found to be approximately 217°C at the inner region of the flat plate (i.e., point A) since the internal heat generation plays a more important role at the inner regions as compared to the outer regions.

Surrogate Model: Kriging

Kriging is a well-known surrogate technique that is frequently used to approximate computationally expensive functions in the course of optimization. The method, named after a South African geologist Krige [23], was developed to estimate mineral concentrations within a particular field and popularized by the work of Sacks et al. [24], which made it also known as Design and Analysis of Computer Experiments. The procedure starts with obtaining a sample data of limited size (i.e., n-design sets each having d-variables), $\boldsymbol{X} = \{\boldsymbol{x}^{(1)}, \boldsymbol{x}^{(2)}, \ldots, \boldsymbol{x}^{(n)}\}^{\mathrm{T}}$, and a corresponding vector of scalar responses $\boldsymbol{y} = \{y^{(1)}, y^{(2)}, \ldots, y^{(n)}\}^{\mathrm{T}}$. It is assumed that if design points, e.g., $\boldsymbol{x}^{(i)}$ and $\boldsymbol{x}^{(j)}$, are positioned close together in the design space, their respective function values $y^{(i)}$ and $y^{(j)}$ are expected to be similar, and vice versa. This can be formulated statistically by considering the correlation between two points as,

$$\mathrm{cor}\left[y\left(x^{(i)}\right), y\left(x^{(j)}\right)\right] = \prod_{k=1}^{d} \exp\left(-\theta_k \left|x_k^{(i)} - x_k^{(j)}\right|^2\right) = \exp\left(-\sum_{k=1}^{d} \theta_k \left|x_k^{(i)} - x_k^{(j)}\right|^2\right) \tag{7}$$

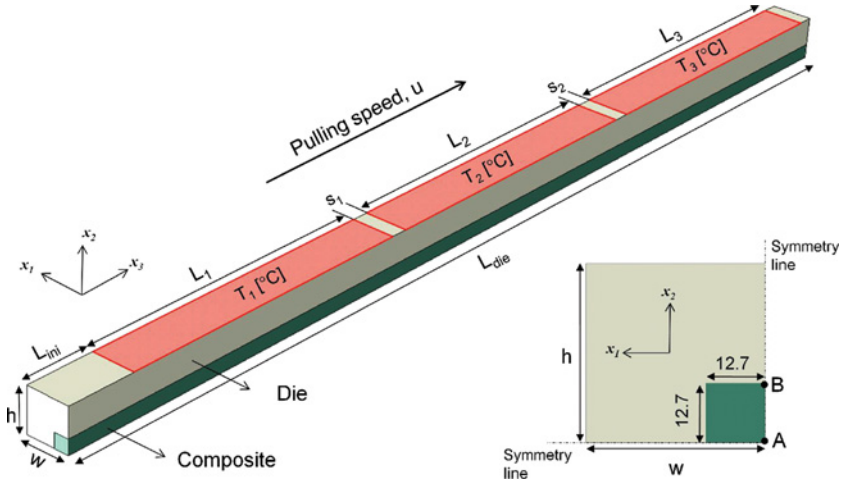

FIGURE 2.—Schematic view of the quarter pultrusion domain.

where θ_k is a correlation parameter or hyperparameter (i.e., $\theta = \{\theta_1, \theta_2, \ldots, \theta_d\}^{\mathrm{T}}$) which controls how fast the correlation changes from one point to the other one along each dimension. Here, Gaussian basis function is used; therefore the exponent is fixed at 2 yielding a smooth and continuous transition at $\boldsymbol{x}^{(i)}$. Equation (7) is used to build the symmetric correlation matrix ($\mathbf{R}$) of all n-points in $\boldsymbol{X}$, which will be used in the process of tuning the unknown hyperparameter θ_k to maximize the likelihood of the assumed Gaussian model on the given dataset. Having the Kriging model parameters tuned, the next step is to predict a new response value, i.e., an objective or a constraint function value, at an unobserved design point using the sample data that are used to train the Kriging model. Ordinary Kriging predictor ($\hat{y}$) has such a form,

$$\hat{y}(\boldsymbol{x}^*) = \hat{\mu} + \boldsymbol{r}(\boldsymbol{x}^*, \boldsymbol{x})^{\mathrm{T}} \boldsymbol{R}(\boldsymbol{x})^{-1} (y(\boldsymbol{x}) - 1\hat{\mu}), \tag{8}$$

where $\boldsymbol{r}(\boldsymbol{x}^*, \boldsymbol{x})$ is the linear vector of correlations between the unknown point to be predicted ($\boldsymbol{x}^*$) and the known sample points ($\boldsymbol{x}$), $\hat{\mu}$ is the estimated mean, and $\mathbf{1}$ is an unit vector of size $n \times 1$. Ordinary Kriging assumes a constant term ($\hat{\mu}$) for the global fitting term in the predictor equation, whereas the universal Kriging uses a known functional form. The second part on the right side of Eq. (8) represents the local deviation from the global term. Kriging is in general known for its good performance in fitting complex functional behavior; however, what makes Kriging a very popular surrogate technique is in essence its ability to estimate the mean squared error (MSE) at the unknown point,

$$\hat{s}^2(x^*) = \hat{\sigma}^2 \left[1 - r^{\mathrm{T}} R^{-1} r + \frac{1 - 1^{\mathrm{T}} R^{-1} r}{1^{\mathrm{T}} R^{-1} 1} \right], \tag{9}$$

where $\hat{s}^2$ represents the MSE estimate. The third term inside the square parentheses is very small and is often neglected. Since Kriging is an interpolation method, $\hat{s}^2$ reduces to zero at the sample points and consequently $\hat{y}$ ecomes equal to the corresponding response value.

TABLE 3.—The details of the parameters (see Fig. 2) used in the thermo-chemical analysis by Chachad et al. [5].

#	Parameter	Description	Value
1	L_{in}	Initial free length	0.06 m
2	L_1	Length of the first heater	0.27 m
3	L_2	Length of the second heater	0.27 m
4	L_3	Length of the third heater	0.27 m
5	S_1	Spacing between the first and second heaters	0.015 m
6	s_2	Spacing between the second and third heaters	0.015 m
7	T_1	Set temperature of the first heater	270°C
8	T_2	Set temperature of the second heater	270°C
9	$T3$	Set temperature of the 3 rd heater	270°C
10	n_{heaters}	Number of heaters	3
11	L_{die}	Length of the die	0.915 m
12	u	Pulling speed	0.0033 m/s
13	$2w$	Width of the die	0.0762 m
14	$2h$	Height of the die	0.0762 m

Efficient Global Optimization (EGO)

Knowing the fact that the Kriging model just constructed on the limited number of sample points (initial sample set) is only an approximation for the underlying black-box function; thus, new sample points (infill points) should iteratively be sought to update or in other words to improve the accuracy of the surrogate. This update procedure, i.e., infill criterion, may consider either only focusing on the optimum region of the predictor (running the risk of premature convergence) or to continue exploring the search space to increase the overall accuracy thereby having a higher probability of finding the global optimum. Another strategy is to balance both efforts, i.e., simultaneously utilizing the information of the predictor $\hat{y}(x)$ calculated by Eq. (8) and the estimation of the variance $s^2(x)$ calculated by Eq. (9). Schonlau [25] and Jones et al. [26] suggested a criterion for their EGO algorithm which is based on improving upon the best sample found so far y_{best}. Recall

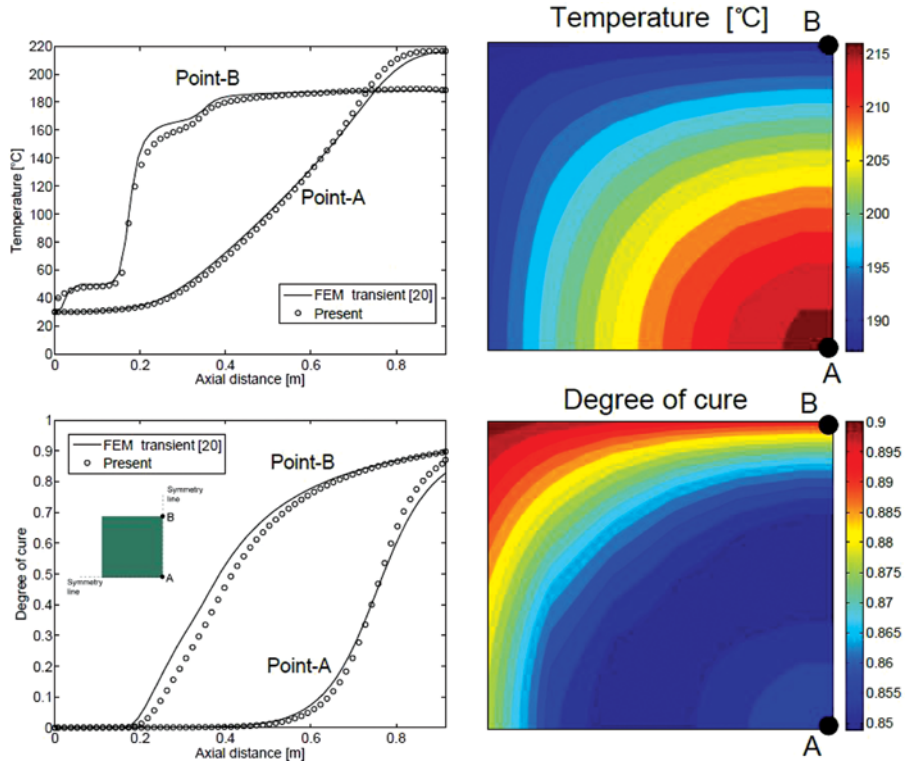

FIGURE 3.—Temperature and degree of cure evolutions inside die for point A and B (left) and the corresponding contour plots at the die exit (at 915 mm from the die inlet) (right).

that the Kriging predictor is the realization of a Gaussian process $Y(\boldsymbol{x})$ with the mean $\hat{y}(\boldsymbol{x})$ and the variance $s^2(x)$; therefore, due to the uncertainty in the predictor, an improvement at a point $\boldsymbol{x}$ can be defined as,

$$I(x) = max(y_{\text{best}} - Y(\boldsymbol{x}), 0), \tag{10}$$

which can be used to maximize the expectation of it (*expected improvement*) as the infill criterion [27, 28],

$$E[I(x)] = (y_{\text{best}} - \hat{y}(\mathbf{x}))\Phi\left(\frac{y_{\text{best}} - \hat{y}(x)}{\hat{s}(x)}\right) + \hat{s}(x)\phi\left(\frac{y_{\text{best}} - \hat{y}(x)}{\hat{s}(x)}\right), \tag{11}$$

where $\Phi(.)$ and $\phi(.)$ are the cumulative distribution function and the probability density function of a normal distribution, respectively. Readers are referred to [29] for the derivation of Eq. (11). EGO iterates until a user-defined stopping criterion is met, e.g., total number of infill points, change in the objective function, tolerance on MSE, etc.

Constrained EGO

The present article introduces a new parameter-less penalty function-like approach into the standard EGO algorithm enabling simultaneously handling of analytical and numerical constraints, some of which have to be satisfied in order to evaluate the performance of designs often occurring in engineering optimization problems. To distinguish these types of constraints from the rest which are calculated without any concern, they are here named as *rigid* constraints, whereas others are named as *flexible* constraints. The particular way of dealing with the rigid constraints in this article avoids the disadvantage associated with the commonly applied intuitive approach, in which those solutions having not-a-number (NaN) flag are disregarded while constructing the surrogate, eventually resulting in loss of valuable information.

The proposed algorithm starts with the calculation of the expected improvement $E[I(\boldsymbol{x})]$ as usual; however, the best solution found so far, y_{best}, is replaced with the current best *feasible* sample response. Then this modified $E[I(\boldsymbol{x})]$ is multiplied with a term called the measure of feasibility, $F(\boldsymbol{x})$, to obtain the *constrained expected improvement* criterion, $E_c[I(\boldsymbol{x})]$, which will eventually be maximized.

$$E_c[I(\boldsymbol{x})] = E[(\boldsymbol{x})]F(\boldsymbol{x}), \tag{12}$$

The measure of feasibility calculated using the corresponding prediction of each constraint function, $\widehat{G}_i(\boldsymbol{x})$, and their constraint limit, $g_{i,\text{limit}}$, is given by

$$F_i(x) = \begin{cases} 0.5 + 0.5\,\text{erf}\left(\frac{\hat{G}_i(x) - g_{i,limit}}{\hat{s}_i(x)}\right), & \text{if erf}\left(\frac{\hat{G}_i(x) - g_{i,\text{limit}}}{\hat{s}_i(x)}\right) \geq 1 \\ 2.0 - \text{erf}\left(\frac{\hat{G}_i(x) - g_{i,\text{limit}}}{\hat{s}_i(x)}\right), & \text{if } 0 < \text{erf}\left(\frac{\hat{G}_i(x) - g_{i,\text{limit}}}{\hat{s}_i(x)}\right) < 1 \\ 0, \text{otherwise} \end{cases} \tag{13}$$

where $\hat{s}_i(\boldsymbol{x})$ is the MSE prediction of i-th constraint function. Figure 4 shows the discontinuous function combining these three conditions.

(i) If all of the constraints are satisfied [first condition in Eq. (13)], i.e., if $\hat{G}_i(\boldsymbol{x}) - g_{i,\text{limit}}$ 0 and $\hat{s}_i(\boldsymbol{x})$ is relatively low, it results in $F_i(\boldsymbol{x}) = 1$. The constrained expected improvement, $E_c[I(\boldsymbol{x})]$, then becomes exactly the same as that for the objective function ($E[I(\boldsymbol{x})]$) alone.
(ii) If all of the constraints are satisfied with an additional condition of at least one of them being very close to the constraint boundary, the second condition in Eq. (13) is applied and an $F_i(\boldsymbol{x})$ value greater than 1 is obtained.
(iii) If any of the constraints is violated or strictly equal to the constraint limit [third condition in Eq. (13)], i.e., if $\hat{G}_i(x) - g_{i,\text{limit}} \leq 0$ without checking any other measure of feasibility for the rest of the constraints, $F_i(\boldsymbol{x})$ is assigned a value 0.

Having the conditions in Eq. (13) explained, $E_c[I(\boldsymbol{x})]$ can either be 0 (i.e., case **(iii)**), $E[I(\boldsymbol{x})]$ (i.e., case **(i)**), or $E[I(\boldsymbol{x})]$ multiplied with a scalar $F_i(\boldsymbol{x}) > 1$ (i.e., case **(ii)**) which provides that particular solution a higher probability of being selected in the process of $\max(E_c[I(\boldsymbol{x})])$. In other words, an infeasible solution has a zero expected improvement function value, a feasible solution closer to the constraint limit is preferred due to the common experience that the optimum solution in general lies on the constraint boundary in engineering design problems, and a feasible solution well inside the feasible search region has an identical expected improvement function value as that of the objective function alone. This preference also provides the advantage of updating the most critical regions of the surrogate of the constraint in a faster manner.

As expected, there is no need for constructing a surrogate for an analytical function, because it is cheap to evaluate; however, there are some special cases to be considered while dealing with analytical constraints in the current implementation of the surrogate-based optimization algorithm,

1. Since they are directly calculated (i.e., there is no uncertainty, $\hat{s}_i(\boldsymbol{x}) = 0), F_i(\boldsymbol{x})$ can either be 1 (case **(i)**) or 0 (case **(iii)**).
2. If the analytical constraint being considered is a rigid constraint and is not satisfied, the infeasible design $\boldsymbol{x}_{\text{infeasible}}$ is altered with the standard binary-coded genetic algorithm (GA) that is also used for the optimization of $E_c[I(\mathbf{x})]$. Instead of starting with a random solution, the infeasible solution is replaced with $\boldsymbol{x}_{\text{best}}$, which is the current best feasible design vector, and is then modified in a specific manner: the individual design variables of $\boldsymbol{x}_{\text{best}}$ which are used in that particular analytical rigid constraint are kept the same (i.e., the rigid constraint is automatically satisfied), but the rest of the variables are perturbed with the GA operators to provide a diversity. It should be kept in mind that, in this way, only the analytical rigid constraints (such as geometrical constraints) are ensured to be satisfied and the analytical or numerical flexible constraints (such as constraints related to a process response) are evaluated in the usual way formulated via Eq. (13). This safety issue can occur either at the execution of the initial sampling plan or during the maximization of the constrained expected improvement function; therefore, this procedure is added wherever it is necessary in the constrained EGO methodology.

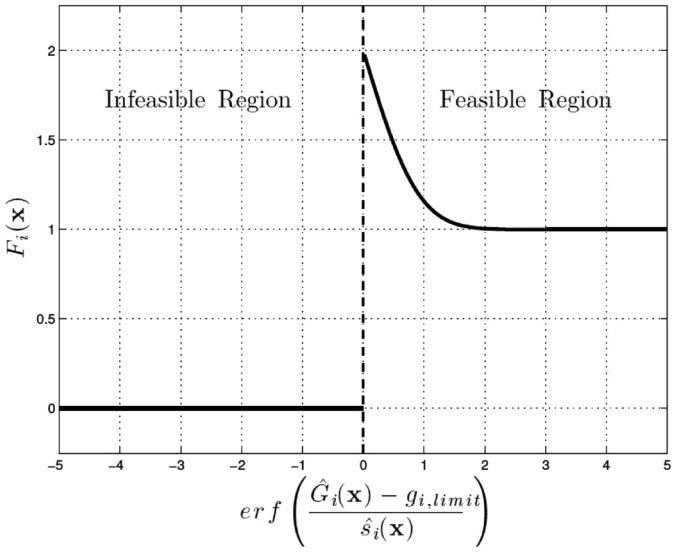

FIGURE 4.—Feasibility function $F_i(\boldsymbol{x})$.

Description of the Optimization Problem

There are a limited number of studies in the numerical optimization aspects of the pultrusion process. These limitations can in general be related to the nature of the multidisciplinary physics and interactions between them involved in the process simulation or the challenges in the field of numerical optimization [11]. The more physics involved with the use of integrated models, the more set of parameters need to be considered for the optimization procedure. Current attempts in optimizing manufacturing processes (based on simulations) with the design of experiments techniques will eventually be replaced or extended by the automated and/or interactive optimization procedures due to the need for efficient way of calculation of immense number of parameter combinations. However, even though these optimization methodologies are efficient in an algorithmic point of view, they may still suffer from the computing time spent to evaluate the objective and constraint function values extracted from the multidisciplinary computer models.

In this section, the optimization problem that the manufacturers often have to deal with in the pultrusion process is briefly described, and the mathematical formulation concerning the thermochemical aspects of the process is presented. It is in essence a scalable problem where the number of unknowns varies depending on a

particular design variable, i.e., the number of heaters ($n_{\text{heaters}} = 1$, 2, or 3) used on the heater die configuration. In the most complex case, there are 13 design parameters and these are the length, width, and height of the die (L_{die}, w, and h, respectively); the initial free length (L_{init}); the length of the heating platens ($L_{1,2,3}$), the spacing between the heaters ($s_{1,2}$), the set temperatures of the heaters ($T_{1,2,3}$), and the pulling speed (u) as depicted in Fig. 2. The objective $f(\boldsymbol{x})$ is to maximize the average cure degree in composite at the die exit. This is constrained with a geometrical and a process response-related constraint as well as the side constraints for the design variables resulting in a total of 15 constraints in case three heaters are used. If only one heater is used, the number of unknowns are reduced to 7 (i.e., L_{die}, w, h, L_{init}, L_1, T_1, and u), whereas the number of unknowns increases to 10 in case of two-heater die configuration (i.e., L_{die}, w, h, L_{init}, $L_{1,2}$, s_1, $T_{1,2}$, and u). These three optimization cases are investigated separately in addition to a validation case having only two unknowns (i.e., L_1 and T_1) in order to make it easy to visualize the progress of the constrained EGO algorithm. The geometrical constraint makes sure that the length of the die is bigger than the total length of the initial length, heater, and spacing between the active heaters. It can be realized that this constraint can directly be calculated without the need of a surrogate. At the same time, it is a rigid constraint which has to be satisfied in order to be able to evaluate the objective function value or the other constraint related to the process response, otherwise the simulation code cannot be executed properly. The process-related constraint is defined as follows: the maximum temperature in the composite $T_{\max}$ should not exceed 240°C. This constraint function, which is in this context classified as a flexible constraint, is evaluated with the use of the nonlinear process simulation model that will be replaced with a surrogate model. This is also the case for the objective function related to the average cure degree. The general constrained optimization problem is formulated below:

$$
\begin{aligned}
&\text{Maximize}: f(x) = \alpha_{\text{avg,exit}} \\
&\text{subjectto}: g_1(x) = L_{\text{die}} \geq L_{\text{init}} + \sum_{i=1}^{n_{\text{heaters}}} L_i + \sum_{i=1}^{n_{\text{heaters}}-1} s_i, \\
&\qquad g_2(x) = T_{\max} < 240\,^{\circ}\text{C}, \\
&\qquad g_3(x) = 0.06 \leq L_{\text{init}} < 0.240\,\text{m}, \\
&\qquad g_{4-6}(x) = 0.06 \leq L_1, L_2, L_3 < 0.36\,\text{m}, \\
&\qquad g_{7-8}(x) = 0.015 \leq s_1, s_2 < 0.25\,\text{m}, \\
&\qquad g_{9-11}(x) = 150 \leq T_1, T_2, T_3 < 250\,^{\circ}\text{C}, \\
&\qquad g_{12}(x) = 0.75 \leq L_{\text{die}} < 1.5\,\text{m}, \\
&\qquad g_{13}(x) = 0.0016 \leq u < 0.01\,\text{m/s}, \\
&\qquad g_{14-15}(x) = 0.0454 \leq w, h < 0.2\,\text{m}, \qquad (14)
\end{aligned}
$$

Results and discussions

The results of the constrained design optimization problems related to the pultrusion process are given in detail in the following subsections. First, the validation case with two design variables is introduced. Following this, the results of the three optimization cases (i.e., one-, two-, and three-heater configuration with 7, 10, and 13 design variables, respectively) are presented. The proposed constrained EGO is run five times for each optimization case with a different initial sample set and the best-mean-worst values of these analyses have been recorded. These are then compared with the results obtained using the standard GA that is also used to train the Kriging model and to optimize the constrained expected improvement function. The GA is run three times with two different population sizes in each case to see if it has any effect on the results. It should be noted that the number of generations is chosen as to have the total number of generations being greater than or at least equal to 10 times the number of function evaluations spent by the constrained EGO in each separate problem case. For instance, in the one-heater optimization problem, the initial sample set has been prepared with a total of 35 samples (i.e., five samples per each design variable which results in $5 \times 7 = 35$ number of samples in total) using an optimized Latin hypercube sampling (LHS). Then, 70 infill points (i.e., twice the size of the initial sample set) are iteratively added by the constrained EGO procedure using the infill criterion, which results in a total of $35 + 70 = 105$ true function evaluations or process simulations. The population size and the total number of generations of the GA are set up in a way that the total number of true function evaluations spent by the GA will be at least 10 times the one spent by the constrained EGO (i.e., minimum $105 \times 10 = 1050$). The number of generations is set up as 17 when the population size is 64 (i.e., $17 \times 64 = 1088 > 1050$) and as 11 when the population size is 96 (i.e., $11 \times 96 = 1056 > 1050$). It should also be noted that the population size of the GA is selected as a multiple of 8 due to the available number of processors; therefore it is run in parallel, and however the comparison is made considering the total number of function evaluations, not the computing time. The optimization results for the other two cases are also compared in a similar manner and the results of the GA runs are summarized in Tables 4–6.

Validation Case: Optimization of the Length and Set Temperature of the Heater

The validation case is prepared in order to make it easier to visualize the progress of the constrained EGO algorithm by reducing the number of unknowns to only 2. The other five design parameters in the one-heater die configuration is fixed as $L_{\text{init}} = 0.2\,\text{m}$, $L_{\text{die}} = 1\,\text{m}$, $u = 0.0016\,\text{m/s}$ and w, $h = 0.0454\,\text{m}$. The set temperature (T_1) and the length (L_1) of the first heater are the design parameters, whereas the objective is to maximize the average cure degree in the composite at the die exit ($\alpha_{\text{avg,exit}}$); meanwhile the maximum temperature at any point in the composite ($T_{\max}$) is desired to be kept below 240°C. As a reminder, lower pulling speed indicates that the composite will stay inside the heating die for a longer

TABLE 4.—Summary of the results obtained using the constrained EGO algorithm.

	Best	Mean	Worst
One-Heater Case (7 var., Initial = 35, Infill = 70)	0.9932	0.9925	0.9918
Two-Beater Case (10 var.. Initial = 50, Infill = 100)	0.9962	0.9949	0.9926
Three-Heater Case (13 var.. Initial = 65, Infill = 130)	0.9975	0.9970	0.9967

TABLE 5.—Results of three GA runs for the one-heater optimization.

	Best	Mean	Worst
$\text{Pop}_{size} = 64$, Gen = 17	0.9920	0.99183	0.9917
$\text{Pop}_{size} = 96$,Gen = 11	0.9916	0.99073	0.9896

period, and therefore the temperature distribution will be more uniform, and what is more to the point is that the maximum temperature will be relatively higher as compared to the case in which the pulling speed is higher. The heat input has a directly proportional effect on the temperature field; hence the design parameters T_1 and L_1 should be chosen carefully in order to satisfy the temperature constraint meanwhile maximizing the $\alpha_{\text{avg,exit}}$ (see Fig. 5, left). A simple interpretation of this relationship would indicate that the upper limits of these unknowns would result in the highest cure degree; however the maximum temperature would also reach its maximum value which is above the limit. The response surface to the right in Fig. 5 shows $T_{\max} - 240$, where the level of zero indicates the constraint limit; therefore, the negative values represent the infeasible solutions (figure is rotated for visibility concerns). It should be noted that the geometrical constraint is automatically satisfied for any design set, considering the lower limit of the die length versus the upper limits of the initial spacing and the length of the first heater (i.e., $\max(L_{\text{init}} + L_1) = 0.2 + 0.36 = 0.56\,\text{m} < 0.75\,\text{m}$). This means that there is no need to consider this constraint for the validation case. Two surrogates (i.e., for $\alpha_{\text{avg,exit}}$ and $T_{\max}$) will be built in the surrogate-based design optimization procedure, and moreover the constraint is classified as a flexible constraint where infeasibility condition is allowed.

The surrogate-based optimization procedure starts with preparing an initial sample set having size of $5 \times k$ (i.e., k is the number of design variables). The chosen multiplier coefficient of 5 is up to the user; for instance, Jones et al. [26] had suggested the use of $10 \times k$. In this study, an optimized LHS is used, but it is again up to the user to select any available uniform space-filling sampling strategy. The distribution of 10 samples is shown in Fig. 6 (left) with bold black circles. The Kriging models of both the objective ($\alpha_{\text{avg,exit}}$) and constraint ($T_{\max}$) functions are constructed upon these 10 design samples at the beginning of the optimization procedure. As expected, the initial fitting is not very accurate; the change in the contour lines can be seen by comparing with the one built at the last stage of the optimization procedure (Fig. 11 (left)). According to Fig. 6 (left), the current optimum of the surrogate built for the objective function lies roughly at somewhere $[L_1,\ T_1] = [0.25,\ 240]$, which is away from the true optimum $[L_1^*,\ T_1^*]$ [0.36, 231.08]. The bold black contour line drawn in Figs. 6–11 indicates the constraint limit (i.e., of the surrogate of $T_{\max}$ constraint), of which the upper design area is infeasible. Therefore, referring to Fig. 6, there is only one infeasible solution in the initial sample set. The surrogate models constructed for the objective and the constraint functions are used within the constrained EGO framework (i.e., by maximizing the constrained expected improvement criterion plotted to the right in Figs. 6–11) to find out where to add the next infill point. At the same time, the unconstrained standard $E[I(\boldsymbol{x})]$ function [Eq. (11)] is also plotted next to the constrained $E[I(\boldsymbol{x})]$, i.e., middle graphs in Figs. 6–11, in order to show the effect of the constraint handling strategy. The optimum locations of the standard $E[I(\boldsymbol{x})]$ and the constrained one are indicated by a red marker in these figures. As clearly seen, the optimum of the unconstrained $E[I(\boldsymbol{x})]$ lies in the infeasible region. The maximization of the constrained $E[I(\boldsymbol{x})]$ computed using the initial sample set gives the new update point as $[L_1^1,\ T_1^1] = [0.273,\ 223.83]$ (see Fig. 6 (right)). This infill point, marked with the bold square ("1") in Fig. 7 (left), is used to update the Kriging models of the objective and constraint functions. The change in the contour lines, especially the one representing the constraint limit, can be seen in the same figure. The new infill point ("2") is again sought by maximizing the constrained $E[I(\boldsymbol{x})]$ function drawn in Fig. 7 (right). This update loop continues until the user-defined tolerance of 0.0001 for the constrained $E[I(\boldsymbol{x})]$ value is met. Due to the limitation of the space, some of the update steps are not shown here. Figure 11 shows the last stage of the update procedure where the exact optimum is found after seven infill points, and the contour lines of the surrogate function surfaces captured the form of the original functions especially in the region where the global optimum lies.

Even though the objective space is not multimodal, it is difficult to find the global optimum since it lies in a wide flat region, like in the case for the well-known Rosenbrock function. A gradient-based mathematical programming algorithm, the sequential quadratic programming (i.e., `fmincon` function in MATLAB [30]) was used for test purposes and it got stuck on any arbitrary point along the contour line of the constraint limit depending on the randomly chosen multiple starting points provided by the user. However, the proposed algorithm found the exact global optimum in each run with different initial sample set. This supports how

TABLE 6.—Results of three GA runs for the two-heater optimization.

	Best	Mean	Worst
$\text{Pop}_{size} = 64$, Gen = 24	0.9963	0.99612	0.9960
$\text{Pop}_{size} = 96$,Gen = 16	0.9962	0.99603	0.9959

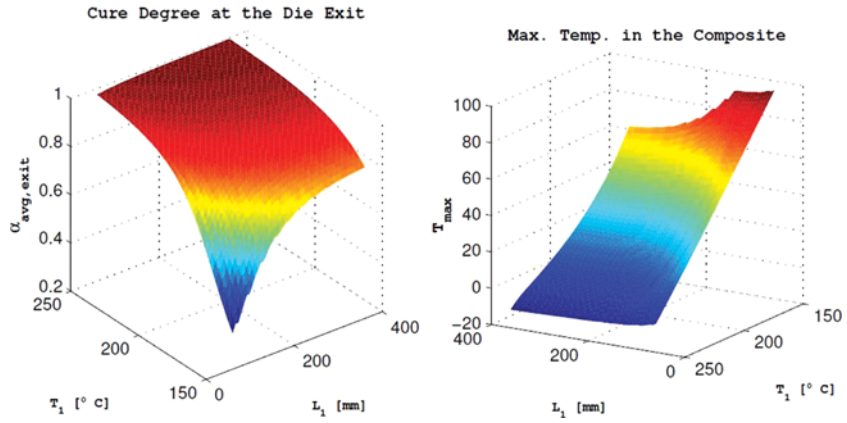

FIGURE 5.—(Left) Validation case: Surface plot of the cure degree at the die exit ($\alpha_{avg,exit}$) as a function of L_1 and T_1. (Right) Validation case: Surface plot of the maximum temperature in the composite (T_{max}) as a function of L_1 and T_1.

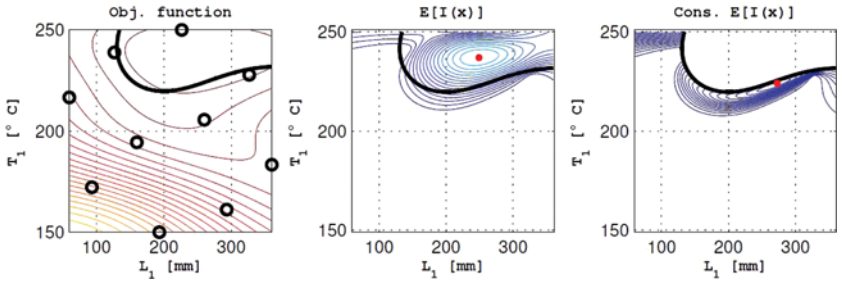

FIGURE 6.—Validation case: The surrogates of the objective (a) and constraint (b) functions built on the initial sample data (circles) determined with the LHS.

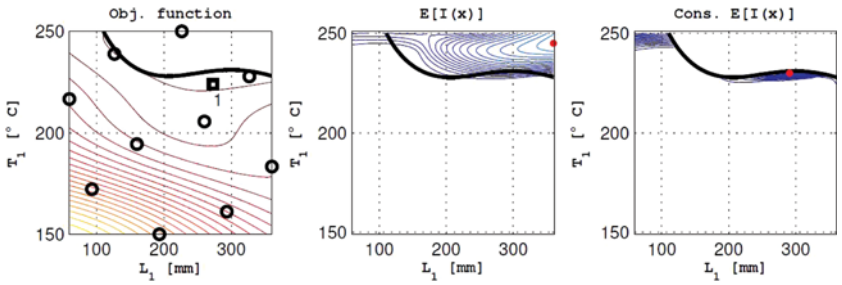

FIGURE 7.—Validation case: Updated surrogate functions of the objective and constraint functions after one infill point (shown with the square).

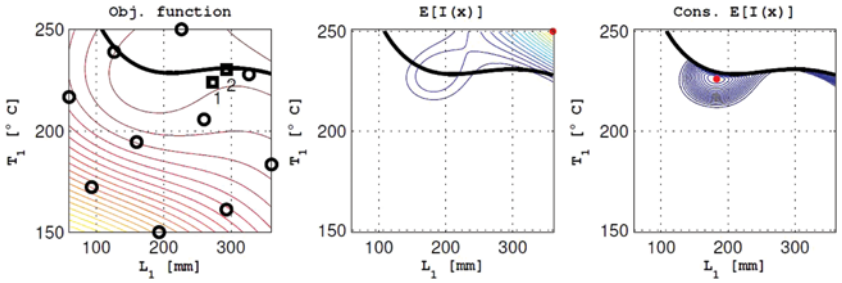

FIGURE 8.—Validation case: Updated surrogate functions of the objective and constraint functions after two infill points (shown with the square).

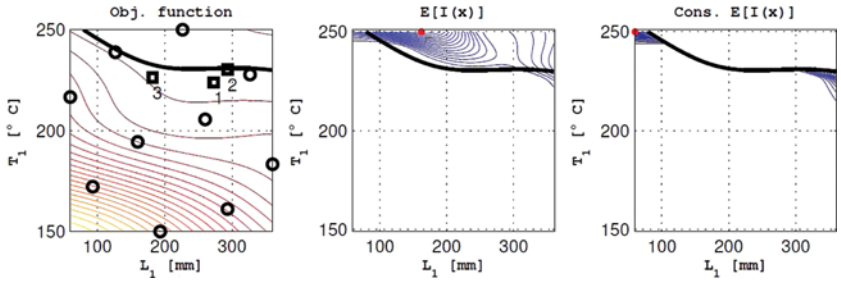

FIGURE 9.—Validation case: Updated surrogate functions of the objective and constraint functions after three infill points (shown with the square).

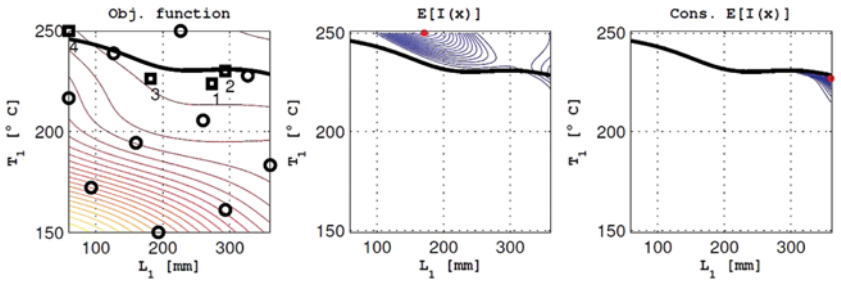

FIGURE 10.—Validation case: Updated surrogate functions of the objective and constraint functions after four infill points (shown with the square).

efficient and robust the proposed methodology is. It should also be noted that, in order to be able to fairly evaluate the performance of the procedure, the distance of the visited points to the global optimum should also be kept in mind while keeping an eye on the progress of the decrease in the objective function. In such a flat region, the overall improvement in the objective function may be very low; however, the global optimum may lie far from the current location.

In the following three sections, the main optimization cases are presented. Due to the high number of variables, the visualization is not possible and the location of the global optimum is not predictable due to the higher order of complexity in the process model and the design problem. Therefore, the results of the proposed constrained $E[I(\boldsymbol{x})]$ algorithm are compared with multiple runs of the standard binary-coded GA that is also used in the surrogate-based optimization procedure.

Optimization Case 1: One-Heater Configuration

In this section, the optimization results of the one-heater die configuration used for the pultrusion process considering seven variables (L_{init}, L_1, T_1, L_{die}, u, w, and h) are given. The initial sample set is prepared with 35 design sets and 70 more are added along the optimization procedure. The progress of the optimization, i.e., the cure degree versus iterations, is shown in Fig. 12. Feasible solutions are depicted by circles, whereas the infeasible solutions are drawn with crosses. The initial sampling set is separated with the dashed line. The global optimum, $\max(\alpha_{\text{avg,exit}})$, is indicated with (-.) line. It should be recalled that even though the objective values of the feasible solutions are close to each other, the global optimum is found at the 91st iteration out of 105 iterations (i.e., 105 true function evaluations or compute-heavy process simulations). In order to have more confidence about the convergence of the algorithm, this proposed algorithm

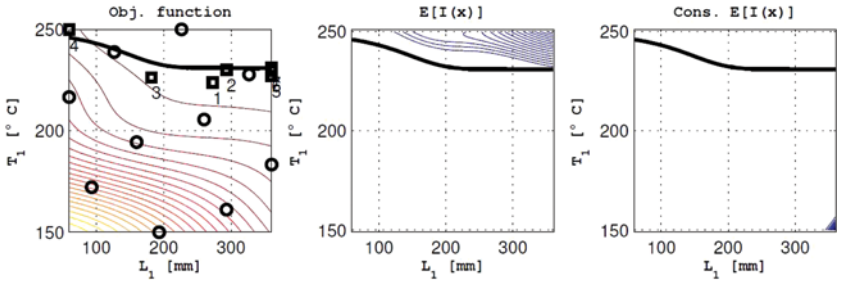

FIGURE 11.—Validation case: Last update on the surrogates of the objective and constraint functions after seven infill points (shown with the square). Optimum solution is, after seven infill points (total of 17 high-fidelity model runs), $[L_1, T_1] = [360\,\text{mm}, 231.02^\circ\text{C}]$. Stopping tolerance is 0.0001.

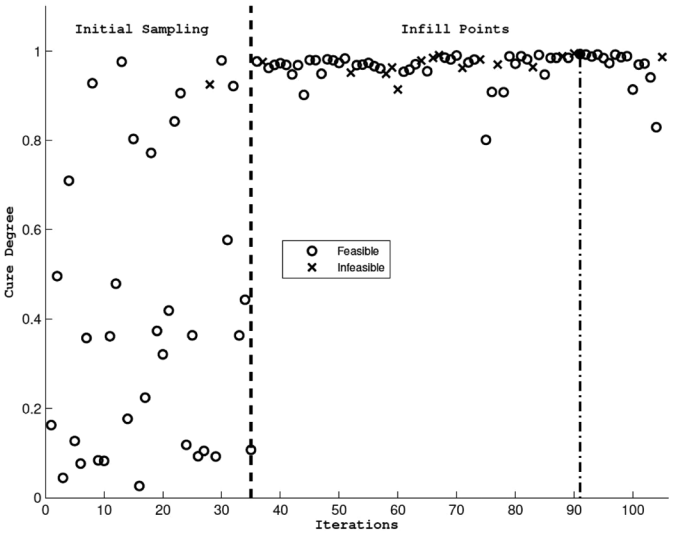

FIGURE 12.—One-heater optimization case (seven variables, 105 iterations). (-.) indicates the best solution which is $(\alpha_{avg,exit})_{best} = 0.9932$ and found at the 91st iteration at third run. $(\alpha_{avg,exit})_{mean} = 0.9925$, $(\alpha_{avg,exit})_{worst} = 0.9918$ in a total of five constrained EGO runs.

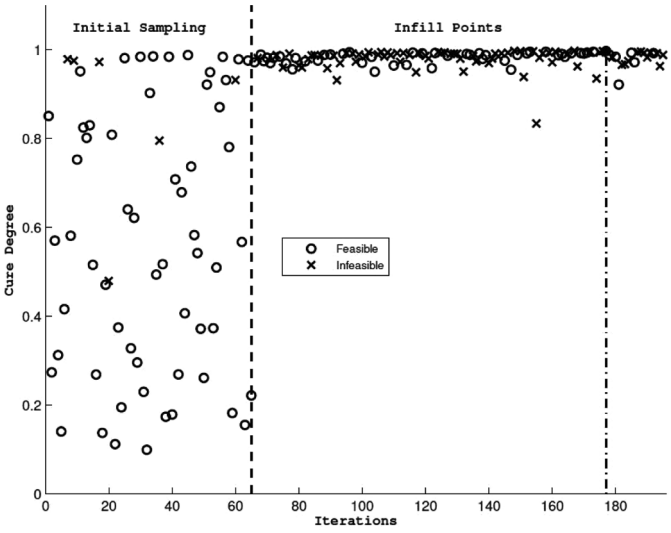

FIGURE 14.—Three-heater optimization case (13 variables, 195 iterations). (-.) indicates the best solution which is $(\alpha_{avg,exit})_{best} = 0.9975$ and found at the 177th iteration at the third run. $(\alpha_{avg,exit})_{mean} = 0.9970$, $(\alpha_{avg,exit})_{worst} = 0.9967$ in a total of five constrained EGO runs.

is executed five times with different initial sample sets, and the results are summarized in the first row of Table 4. Figure 12 shows the progress of the best run listed in the first row of Table 4. The results obtained with the use of the constrained GA (i.e., three runs with different initial populations) are also summarized in Table 5. The criterion for the particular setting of the population size and the total number of generations is explained in the Results and Discussion section. It can be clearly seen that the results obtained using the constrained EGO algorithm is better than those obtained by the constrained GA with only 1/10th of the computational cost (i.e., total number of true function evaluations).

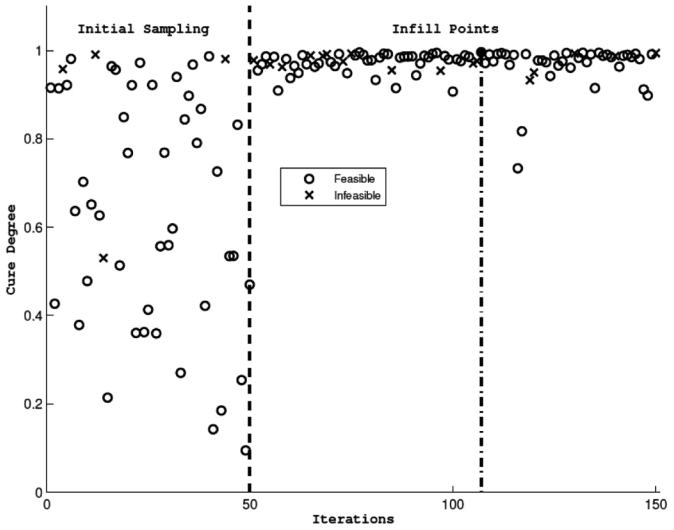

FIGURE 13.—Two-heater optimization case (10 variables, 150 iterations). (-.) indicates the best solution which is $(\alpha_{avg,exit})_{best} = 0.9962$ and found at the 107th iteration at first run. $(\alpha_{avg,exit})_{mean} = 0.9949$, $(\alpha_{avg,exit})_{worst} = 0.9926$ in a total of five constrained EGO runs.

Optimization Case 2: Two-Heater Configuration

The optimization results of the two-heater die configuration used for the pultrusion process considering 10 variables (L_{init}, $L_{1,2}$, s_1, $T_{1,2}$, L_{die}, u, w, and h) are given here. The initial sample set is prepared with 50 design sets and 100 more are added along the optimization procedure. The progress of the optimization is shown in Fig. 13. The global optimum is found at the 107th iteration out of 150 iterations. The results of five different constrained EGO runs are summarized in the second row of Table 4. Figure 13 shows the progress of the best run listed in this row of Table 4. The results obtained with the use of the constrained GA runs (i.e., three runs with each population size) are also summarized in Table 6, and they show a quite similarity which supports the confidence in the proposed methodology. It should be kept in mind that almost the same results are obtained with only 1/10th of the computational cost.

Optimization Case 3: Three-Heater Configuration

In this last optimization case study, the results of the three-heater die configuration used for the pultrusion process considering 13 variables (L_{init}, $L_{1,2,3}$, $s_{1,2}$, $T_{1,2,3}$, L_{die}, u, w, and h) are given. The initial sample set is

TABLE 7.—Results of three GA runs for the three-heater optimization.

	Best	Mean	Worst
$Pop_{size} = 64$, Gen = 31	0.9975	0.9973	0.9971
$Pop_{size} = 96$,Gen = 21	0.9974	0.99711	0.9969

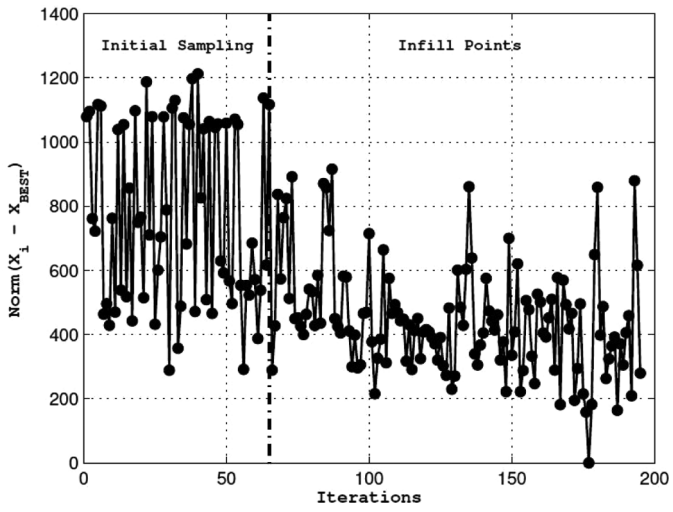

FIGURE 15.—Evolution of the norm for the three-heater optimization problem.

prepared with 65 design sets and 130 more are added along the optimization procedure. The progress of the optimization is shown in Fig. 14. The global optimum is found at the 177th iteration out of 195 iterations. The results of five different constrained EGO runs are summarized in the third row of Table 4. Figure 14 shows the progress of the best run listed in this row of Table 4. The results obtained with the use of the constrained GA are also summarized in Table 7, and they again show negligible difference which supports the confidence in the proposed methodology. Here, in Fig. 15, the distance between each iterative solution ($\boldsymbol{x}_\mathbf{i}$) and the global optimum ($\boldsymbol{x}_\mathbf{best}$) is also drawn in order to show the progress of the algorithm in the design space rather than only the objective space (Fig. 14). At iteration 177, the norm ($\boldsymbol{x}_\mathbf{177} - \boldsymbol{x}_\mathbf{best}$) vanishes because $\boldsymbol{x}_\mathbf{177} = \boldsymbol{x}_\mathbf{best}$.

CONCLUSIONS

In the present work, a steady-state thermochemical simulation of the pultrusion of a thick flat beam has been implemented, validated with the transient solution given in [6, 7], and optimized using a surrogate-based optimization methodology, here called as constrained EGO algorithm. The optimization problem to be solved has a single objective that is to maximize the average cure degree at the exit of the heating die. The problem includes a geometrical and a process-related constraint besides particular parameter bounds. Three different cases for the same optimization problem are considered which also indicates that it is a scalable problem. The number of variables varies in each case due to the geometrical configuration of the heating die, i.e., the number of heaters used, $n_{\text{heaters}} = 1$, 2, and 3, whereas the number of parameters, $n = 7$, 10, and 13. A two-variable optimization case is presented beforehand to make it easier to visualize the progress of the proposed methodology. Findings can be summarized as follows:

1. Due to the compute-heavy nature of the implemented numerical model of the pultrusion process, an approximations or the so-called the surrogates of the objective and constraint functions are constructed. Kriging is chosen as the surrogate model. The procedure starts with an initial set obtained with the optimized LHS. The infill strategy that is using the proposed constrained expected improvement criterion is iteratively applied to update (to improve the accuracy of) the model by simultaneously balancing the exploitation and the exploration concerns.
2. A new parameter-less penalty function-like constraint handling methodology is proposed. The selection of the best response (objective function) value, y_{best}, in Eq. (11) differs in the constrained EGO algorithm in a way that the best feasible objective function value is selected instead of the overall best one.
3. Analytical and numerical constraints are handled together. Since it is very straightforward to evaluate the analytical constraints, surrogates are considered only for the numerical objective and constraint functions.
4. A classification of rigid and flexible constraints is introduced. Rigid constraints are those which have to be satisfied in order to be able to evaluate the corresponding objective or constraint function value of the design under consideration. For instance, as it is encountered in this study, the die length should be bigger than the total length of the active heater lengths, initial die length, and space between the heaters in order to be able to evaluate the temperature field (i.e., as a consequence, the cure degree, $\alpha_{\text{avg,exit}}$, and the maximum temperature at any point in the composite, $T_{\max}$). Instead of directly ignoring such solutions having a flag of NaN, a fast methodology to gain a feasible solution is developed by utilizing the best design vector, $\boldsymbol{x}_\mathbf{best}$. However, this is considered only for the analytical rigid constraint in this particular design problem.
5. The results of the three optimization cases are compared with those obtained with the standard binary-coded GA that is also used to tune the parameters of the surrogate model and to maximize the constrained expected improvement criterion for the infill strategy. Both the surrogate-based procedure and the constrained GA have been run several times with different starting conditions to be statistically sure of the convergence of the results. Finally, it is found that the proposed methodology solves each design problem at a much lower cost, i.e., 1/10th of the total number of true function evaluations (numerical process models) spent by applying a standard global optimization algorithm (GA).

This is a common methodology where the specific surrogate model, Kriging in this case, can be replaced with another approximation model under one circumstance that the estimation of the prediction error should be available in order to compute the constrained expected improvement criterion. An alternative for the Kriging

model, such as the radial basis function or the support vector regression, can be considered due to the fact that it computationally gets heavier at high dimensions to update the model while iteratively computing the inverse of the correlation matrix.

Optimization problems in engineering in general comprise multiple objectives often having conflict with each other. Evolutionary multiobjective optimization algorithms provide an ideal way of solving this type of problems, where multiple solutions are sought in parallel, without any biased treatment of objectives such as weighting constants serving as presumed user preferences. Their population approach provides an advantage of inherent parallel processing capability. However, as expected, this advantage does not come free. Evaluation of multiple objectives and constraints generally requires a larger population size and/or more iterations. This obviously means more function evaluations, which again emphasizes the need for an efficient surrogate-based optimization methodology for especially the simulation-based multiobjective optimization problems in engineering design.

Although we shall investigate these aspects next, the current study makes a significant contribution in developing and applying a surrogate-based design optimization method for a practical manufacturing problem in the pultrusion industry.

Funding

The authors wish to acknowledge the funding support provided by the Department of Electrical and Computer Engineering, Michigan State University, for executing this study.

References

1. Hackett, R.M.; Prasad, S.N. Pultrusion process modeling. *Advances in Thermoplastic Matrix Composite Materials ASTM STP* **1989**, *1044*, 62–70.
2. Ding, Z.; Li, S.; Lee, L.J. Influence of heat transfer and curing on the quality of pultruded composites II: Modeling and simulation. *Polymer Composites* **2002**, *23*, 957–969.
3. Carlone, P.; Palazzo, G.S.; Pasquino, R. Pultrusion manufacturing process development by computational modelling and methods. *Mathematical and Computer Modelling* **2006**, *44*, 701–709.
4. Valliappan, M.; Roux, J.A.; Vaughan, J.G.; Arafat, E.S. Die and post-die temperature and cure in graphite-epoxy composites. *Composites Part B: Engineering* **1996**, *27*, 1–9.
5. Chachad, Y.R.; Roux, J.A.; Vaughan, J.G.; Arafat, E.S. Three-dimensional characterization of pultruded fiberglass-epoxy composite materials. *Journal of Reinforced Plastics and Composites* **1995**, *14*, 495–512.
6. Baran, I.; Tutum, C.C.; Hattel, J.H. The effect of thermal contact resistance on the thermosetting pultrusion process. *Composites Part B: Engineering* **2013**, *45*, 995–1000.
7. Baran, I.; Hattel, J.H.; Tutum, C.C. Thermo-chemical modelling strategies for the pultrusion process. *Applied Composite Materials* **2013**, *20*, 1247–1263.
8. Baran, I.; Tutum, C.C.; Nielsen, M.W.; Hattel, J.H. Process induced residual stresses and distortions in pultrusion. *Composites Part B: Engineering* **2013**, *51*, 148–161.
9. Baran, I.; Tutum, C.C.; Hattel, J.H. Optimization of the thermosetting pultrusion process by using hybrid and mixed integer genetic algorithms. *Applied Composite Materials* **2013**, *20*, 449–463.
10. Tutum, C.C.; Baran, I.; Deb, K. Optimum design of pultrusion process via evolutionary multi-objective optimization. *International Journal Advanced Manufacturing Technology* **2014**, *72*, 1205–1217.
11. Tutum, C.C.; Hattel, J.H. State-of-the-art multi-objective optimisation of manufacturing processes based on thermo-mechanical simulations. In *Multi-Objective Evolutionary Optimisation for Product Design and Manufacturing*; Springer: New York, 2011; 71–133.
12. Haftka, R.T. Combining global and local approximations. *AIAA Journal* **1991**, *29* (9), 1523–1525.
13. Jin, Y. A comprehensive survey of fitness approximation in evolutionary computation. *Journal of Soft Computing* **2005**, *9* (1), 3–12.
14. Queipo, N.V.; Haftka, R.T.; Shyy, W.; Goel, T.; Vaidyanathan, R.; Tucker, P.K. Surrogate-based analysis and optimization. *Progress in Aerospace Sciences* **2005**, *41*, 1–28.
15. Simpson, T.W.; Toropov, V.; Balabanov, V.; Viana, F.A.C. Design and analysis of computer experiments in multidisciplinary design optimization: A review of how far we have come - or not. In *12th AIAA/ISSMO Multidisciplinary Analysis and Optimization Conference*, Victoria, British Colombia, 2008.
16. Giri, B.K.; Hakanen, J.; Miettinen, K.; Chakraborti, N. Genetic programming through bi-objective genetic algorithms with a study of a simulated moving bed process involving multiple objectives. *Applied Soft Computing* **2013**, *13* (5), 2613–2623.
17. Govindan, D.; Chakraborty, S.; Chakraborti, N. Analyzing the fluid flow in continuous casting through evolutionary neural nets and multi-objective genetic algorithms. *Steel Research International* **2010**, *81*, 197–203.
18. Mondal, D.N.; Sarangi, K.; Pettersson, F.; Sen, P.K.; Saxen, H.; Chakraborti, N. Cu-Zn separation by supported liquid membrane analyzed through multi-objective genetic algorithms. *Hydrometallurgy* **2011**, *107*, 112–123.
19. Pettersson, F.; Chakraborti, N.; Saxen, H. A genetic algorithms based multi-objective neural net applied to noisy blast furnace data. *Applied Soft Computing* **2007**, *7*, 387–397.
20. Forrester, A.I.J.; Sobester, A.; Keane, A.J. *Engineering Design Via Surrogate Modelling: A Practical Guide*; Wiley: Chichester, UK, 2008.
21. Jones, D.R.; Schonlau, M.; Welch, W.J. Efficient global optimization of expensive black-box functions. *Journal of Global Optimization* **1998**, *13*, 455–492.
22. Liu, X.L.; Crouch, I.G.; Lam, Y.C. Simulation of heat transfer and cure in pultrusion with a general-purpose finite element package. *Composites Science and Technology* **2000**, *60*, 857–864.
23. Krige, D. A statistical approach to some basic mine valuation problems on the Witwatersrand. *Journal of the Chemical, Metallurgical and Mining Society of South Africa* **1951**, *52* (6), 119–139.
24. Sacks, J.; Welch, W.J.; Mitchell, T.J.; Wynn, H.P. Design and analysis of computer experiments. *Statistical Science* **1989**, *4*, 409–423.

25. Schonlau, M. Computer experiments and global optimization. PhD dissertation, University of Waterloo, Waterloo, Ontario, Canada, 1997.
26. Jones, D.R.; Schonlau, M.; Welch, W.J. Efficient global optimization of expensive black-box functions. *Journal of Global Optimization* **1998**, *13*, 455–492.
27. Viana, F.; Haftka, R.; Steffen, V. Multiple surrogates: How cross-validation errors can helps us to obtain the best predictor. *Structural and Multidisciplinary Optimization* **2009**, *39* (4), 439–457.
28. Sasena, M.J. Flexibility and efficiency enhancements for constrained global design optimization with Kriging approximations; PhD dissertation, University of Michigan, Ann Arbor, Michigan, USA, 2002.
29. Viana, F.A.C. Multiple surrogates for prediction and optimization; PhD dissertation, University of Florida, Gainesville, Florida, USA, 2011.
30. Branch, M.A.; Grace, A. *Optimization Toolbox User's Guide, Version 2*. The Math Works Inc. http://www.mathworks.com/help/pdf_doc/optim/optim_tb.pdf